J Biomol NMR
DOI 10.1007/s10858-017-0124-7

ARTICLE

^{2}H–^{13}C correlation solid-state NMR for investigating dynamics and water accessibilities of proteins and carbohydrates

Martin D. Gelenter[1] · Tuo Wang[1] · Shu-Yu Liao[1] · Hugh O'Neill[2] · Mei Hong[1]

Received: 4 May 2017 / Accepted: 29 June 2017

Abstract Site-specific determination of molecular motion and water accessibility by indirect detection of ^{2}H NMR spectra has advantages over dipolar-coupling based techniques due to the large quadrupolar couplings and the ensuing high angular resolution. Recently, a Rotor Echo Short Pulse IRrAdiaTION mediated cross polarization ($^{\text{RESPIRATION}}$CP) technique was developed, which allowed efficient transfer of ^{2}H magnetization to ^{13}C at moderate ^{2}H radiofrequency field strengths available on most commercial MAS probes. In this work, we investigate the ^{2}H–^{13}C magnetization transfer characteristics of one-bond perdeuterated CD_n spin systems and two-bond H/D exchanged C–(O)–D and C–(N)–D spin systems in carbohydrates and proteins. Our results show that multi-bond, broadband ^{2}H–^{13}C polarization transfer can be achieved using ^{2}H radiofrequency fields of ~50 kHz, relatively short contact times of 1.3–1.7 ms, and with sufficiently high sensitivity to enable 2D ^{2}H–^{13}C correlation experiments with undistorted ^{2}H spectra in the indirect dimension. To demonstrate the utility of this ^{2}H–^{13}C technique for studying molecular motion, we show ^{2}H–^{13}C correlation spectra of perdeuterated bacterial cellulose, whose surface glucan chains exhibit a motionally averaged C6 ^{2}H quadrupolar coupling that indicates fast *trans-gauche* isomerization about the C5–C6 bond. In comparison, the interior chains in the microfibril core are fully immobilized. Application of the ^{2}H–^{13}C correlation experiment to H/D exchanged *Arabidopsis* primary cell walls show that the O–D quadrupolar spectra of the highest polysaccharide peaks can be fit to a two-component model, in which 74% of the spectral intensity, assigned to cellulose, has a near-rigid-limit coupling, while 26% of the intensity, assigned to matrix polysaccharides, has a weakened coupling of 50 kHz. The latter O–D quadrupolar order parameter of 0.22 is significantly smaller than previously reported C–D dipolar order parameters of 0.46–0.55 for pectins, suggesting that additional motions exist at the C–O bonds in the wall polysaccharides. ^{2}H–^{13}C polarization transfer profiles are also compared between statistically deuterated and H/D exchanged GB1.

Keywords Molecular motion · $^{\text{RESPIRATION}}$CP · Cellulose · Plant primary cell walls · *Trans-gauche* isomerization

Introduction

Deuterium is an extremely informative but underutilized spin in biological solid-state NMR (SSNMR). As a spin-1 nucleus, the ^{2}H quadrupole moment couples with local electric field gradients to produce inhomogeneously broadened spectra whose quadrupolar coupling constant (C_Q) and asymmetry parameter (η) reflect the local electronic structure. C–D and O–D groups in organic molecules have large rigid-limit C_Q values of 170–300 kHz (Hunt and MaCkay 1974), with the main principal axis along the bond. Thus ^{2}H quadrupolar spectra are extremely sensitive to molecular orientation and motion, but at the same time have low sensitivity and site resolution. So far, motional amplitudes are most commonly measured through ^{13}C–^{1}H or ^{15}N–^{1}H dipolar couplings using the dipolar-chemical-shift (DIPSHIFT) correlation approach (Munowitz et al. 1981). This family of

✉ Mei Hong
meihong@mit.edu

[1] Department of Chemistry, Massachusetts Institute of Technology, Cambridge, MA 02139, USA

[2] Center for Structural Molecular Biology, Oak Ridge National Laboratory, Oak Ridge, TN 37831, USA

Published online: 03 July 2017

separated-local-field techniques has site resolution through ^{13}C or ^{15}N chemical shifts and relatively high sensitivity since the magnetization originates readily from protons. However, the one-bond ^{13}C–^{1}H and ^{15}N–^{1}H dipolar couplings have relatively small rigid-limit values of 22.7 and 10.8 kHz, respectively. As the static magnetic field strength continues to increase for modern solid-state NMR, the magic-angle-spinning (MAS) frequency also increases proportionally to average the chemical shift anisotropy (CSA). As a result, the DIPSHIFT approach of sampling the dipolar anisotropy within a rotor period becomes increasingly less sensitive to large-amplitude molecular motions with small order parameters. Dipolar coupling amplification techniques (Cobo et al. 2012; Hong et al. 1997) have been proposed to overcome this limitation, but the larger number of pulses reduces the accuracy of the measured couplings. Active heteronuclear recoupling using R-symmetry pulse sequences (Hou et al. 2011; Lu et al. 2016) were recently introduced to measure dipolar couplings at ~40 kHz MAS. Although this approach gives well-resolved splittings for couplings near the rigid limit, its utility for measuring very small, motionally averaged, dipolar couplings has yet to be demonstrated.

In comparison, the large size of the ^{2}H quadrupolar interaction makes it a natural probe of large-amplitude molecular motions and small order parameters. Moreover, the increasing use of perdeuterated proteins and other biomolecules for ^{1}H-detected structure determination experiments (Andreas et al. 2015; Reif 2012) makes it efficient to characterize molecular motions using the same samples. To obtain ^{2}H quadrupolar spectra with site resolution, indirect detection of ^{2}H spectra through ^{13}C and/or ^{15}N is necessary, which requires coherence transfer from ^{2}H to ^{13}C/^{15}N (Hologne et al. 2005). However, simple ^{2}H–^{13}C Hartman–Hahn cross polarization (CP) (Pines et al. 1972) following ^{2}H excitation cannot be readily applied since most commercial triple-resonance ^{1}H/^{2}H/^{13}C MAS probes do not permit ^{2}H radiofrequency (rf) field strengths of more than 50 kHz, which is significantly weaker than the rigid-limit ^{2}H quadrupolar couplings and only comparable to methyl rotation-averaged couplings. With moderate rf fields, the effective field experienced by ^{2}H spins is highly sensitive to crystallite orientations and C_Q values, thus reducing the coherence transfer efficiency and distorting the indirectly detected ^{2}H spectra. Furthermore, simulations show that even strong rf field strengths cannot simultaneously transfer magnetization between rigid and mobile ^{2}H–^{13}C moieties simultaneously due to the strong dependence of CP matching conditions on C_Q (Jain et al. 2014). Recently, Nielsen and coworkers overcame this problem by developing a Rotor Echo Short Pulse IRrAdiaTION mediated CP ($^{\text{RESPIRATION}}$CP) technique (Jain et al. 2012; Wei et al. 2011) in which a series of short rotor-synchronized rf pulses of variable flip angles on the two channels are intertwined with phase-alternated continuous-wave recoupling pulses on one of the two channels. By applying the weak ^{13}C recoupling pulses at rf field strengths that are 1–2 times the MAS frequencies, the ^{2}H channel experiences only the strong and short rotor-echo pulses (Fig. 1). The average Hamiltonian for $^{\text{RESPIRATION}}$CP for a short pulse flip angle of 90° and a recoupling field of $\omega_1 = 2\omega_r$ includes both first- and second-order Fourier components of the ^{2}H–^{13}C dipolar coupling and depends on both the β and γ angles of the C–D vector with respect to the rotor axis (Jain et al. 2012), which results in more efficient coherence transfer than γ-encoded sequences such as Hartman–Hahn CP (Nielsen et al. 1994).

^{2}H–^{13}C $^{\text{RESPIRATION}}$CP following multi-pulse RESPIRATION excitation of the ^{2}H magnetization was first used for resonance assignment of perdeuterated proteins (Akbey et al. 2014). Recently, Rienstra and coworkers incorporated adiabatic $^{\text{RESPIRATION}}$CP into a 3D ^{2}H–^{13}C–^{13}C correlation experiment to measure motionally averaged ^{2}H quadrupolar spectra in a site-specific manner (Shi and Rienstra 2016). Using uniformly ^{13}C, ^{2}H, ^{15}N (CDN)-labeled GB1 with 10% back-exchanged protons as the model system, they showed that the 2D ^{13}C–^{13}C plane resolves nearly all ^{13}C signals while the ^{2}H dimension yielded both motionally averaged quadrupolar coupling constants ($\overline{C_Q}$) and asymmetry parameters ($\overline{\eta}$).

In principle, this $^{\text{RESPIRATION}}$CP ^{2}H–^{13}C correlation approach can be applied not only to perdeuterated proteins but also to perdeuterated carbohydrates and other biomolecules. In addition, the deuterons can be introduced not only at CH_n groups during protein expression but also by simple H/D exchange of labile hydrogens. The latter can not only reveal dynamics of O–D, N–D and S–D groups but also probe water accessibilities of many chemically important polar sidechains such as Thr, Ser, Asp, Glu, Arg and Lys in proteins. ^{2}H–^{13}C correlation of such H/D exchanged samples may also present opportunities for spectral editing to reduce spectral congestion and facilitate resonance assignment. This would complement other spectral editing NMR approaches based on the number of attached protons,

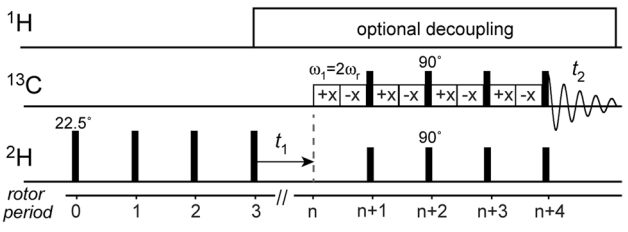

Fig. 1 2D ^{2}H–^{13}C correlation pulse sequence, involving ^{2}H RESPIRATION excitation, ^{2}H t_1 evolution, $^{\text{RESPIRATION}}$CP from ^{2}H to ^{13}C, and ^{13}C detection

the presence of bonded nitrogen, and chemical shift anisotropies (Frey and Opella 1984; Lesage et al. 1998; Mao and Schmidt-Rohr 2004, 2005; Schmidt-Rohr et al. 2012; Schmidt-Rohr and Mao 2002; Williams et al. 2015; Wu et al. 1994).

In this work, we examine polarization transfer efficiencies of ^{RESPIRATION}CP for one- and two-bond ^{2}H–^{13}C spin pairs and demonstrate the application of 2D ^{2}H–^{13}C correlation NMR to a range of perdeuterated and H/D exchanged molecular systems, including amino acids, glucose, bacterial cellulose, plant cell walls, and GB1. SSNMR has recently been used to great effect to characterize the structure and dynamics of polysaccharides in plant cell walls. Several important model plants, including *Arabidopsis thaliana, Brachypodium distachyon* and *Zea mays*, have been enriched with ^{13}C and subjected to 2D and 3D ^{13}C–^{13}C and ^{1}H–^{13}C correlation experiments to understand how intermolecular contacts and polysaccharide motion explain cell wall biomechanical properties (Dick-Perez et al. 2012; Komatsu and Kikuchi 2013; Wang et al. 2014, 2015, 2016a, b; White et al. 2014). These studies have examined wall polysaccharide dynamics using ^{13}C–^{1}H DIPSHIFT experiments and relaxation NMR (Dick-Pérez et al. 2011; Wang et al. 2015, b, 2016a), showing that matrix polysaccharides exhibit large-amplitude motion. However, the highly abundant hydroxyl groups in these carbohydrates have not been probed. The current study provides new information about polysaccharide motions and water accessibilities in these plant cell walls.

Materials and methods

Sample preparation

Several carbohydrates and proteins with different deuteration schemes and deuteration levels are employed in this study. Methyl-deuterated and ^{13}C natural abundance Ala and ^{13}C,^{2}H,^{15}N (CDN)-labeled Val were purchased from Cambridge Isotope Laboratories (Andover, MA). Dry powders of these samples were packed into 3.2 and 4 mm MAS rotors without further purification. 50 mg of protonated and ^{13}C-labeled D-glucose was exchanged with D_2O by dissolution in 250 µL of 70% D_2O. The solution was heated at 50 °C for 1 h and then lyophilized for 4 h. 20 mg of the sample was packed into a 3.2 mm MAS rotor.

Uniformly ^{13}C, ^{2}H-labeled bacterial cellulose was produced from *Acetobacter xylinus* sub sp. *sucrofermentans* (ATCC 700178) and purified using a previously published procedure (Bali et al. 2013; He et al. 2014). The growth medium contained ~98% D_2O with U-$^{13}C_6$ and 1,2,3,4,5,6,6-D_7 labeled D-glucose as the sole carbon source. After 2 weeks of growth at room temperature, the cellulose pellicles were frozen at −20 °C and ground to a slurry using a Waring blender. The bacterial debris was removed by successive washing in 1% NaOD until the A_{280} absorbance was <0.01. Finally, cellulose was neutralized by washing with D_2O until the pH of the surrounding solvent reached ~7.

Protonated and ^{13}C-labeled *Arabidopsis thaliana* primary cell walls were prepared as previously described (Wang et al. 2015; White et al. 2014). About 60 mg of hydrated ^{13}C-labeled cell wall was lyophilized to give ~12 mg of dry material. The dry cell wall was rehydrated with 35 mg D_2O, vortexed and fully mixed, then packed into a 3.2 mm MAS rotor.

^{13}C, ^{15}N-labeled GB1 (CN-GB1) was expressed according to published protocols (Franks et al. 2005) using BL21 (DE3) *E. coli* cells (plasmid kindly provided by Professor Robert Griffin). The protein was purified using a HiLoad 26/60 Superdex 75 prep grade column (GE) using a pH 7.0 phosphate buffer containing 100 mM NaCl. The yield of the purified protein was ~120 mg/L. The GB1-containing column fraction was then dialyzed against 4 L of pH 5.5 phosphate buffer without NaCl to remove NaCl and reach the optimal pH for crystallization. The buffer was changed twice a day for 4 days.

For H/D exchange, the CN-GB1 solution was concentrated to 40 mg/ml using an Amicon Ultra-15 concentrator with a 3 kDa molecular weight cut off (Millipore). 0.5 ml of this solution was exchanged with 3 ml of D_2O buffer and then concentrated to 0.5 ml, giving a deuteration level of ~83%. This solution was exchanged again with 2 ml of D_2O, increasing the deuteration level to ~96%, before being concentrated to 20 mg/ml for crystallization.

To produce microcrystalline protein, 1 ml of the 20 mg/ml H/D exchanged CN-GB1 solution was mixed with three 1 ml aliquots of a crystalizing solution containing 2-methyl-2,4-pentanediol (MPD) and isopropanol (IPA) at a volume ratio of 2:1 to precipitate the crystals. The protein concentration (20 mg/ml) was lower than some of the literature values (Franks et al. 2005; Nadaud et al. 2007; Schmidt et al. 2007) to slow down the crystallization rate and increase the crystal quality. Although the crystallizing MPD and IPA contain exchangeable protons, incubation at 4 °C is expected to slow down H/D exchange. Based on the relative concentrations of D_2O and MPD/IPA in the crystallization solution, the minimum theoretical deuteration level for the exchangeable sites is 70%. Direct measurement of the ^{1}H-^{15}N CP spectra confirmed that the actual deuteration level is ~80% for the exchangeable sites.

Uniformly ^{13}C, ^{15}N- and 70% ^{2}H-labeled GB1 (CDN-GB1) was expressed in a similar fashion as CN-labeled GB1. For optimizing bacterial growth and protein expression in D_2O, bacteria were grown at successively higher D_2O concentrations. A 1 ml aliquot of an H_2O grown

culture was used to inoculate 10 ml of M9 minimal media containing 30% D_2O. 1 ml of this 30% D_2O culture was then used to inoculate 10 ml of M9 containing 50% D_2O. The final stage of training consisted of utilizing 1 ml of the 50% D_2O culture to inoculate 10 ml of M9 containing 70% D_2O (Nand et al. 2012). A 10 ml aliquot of the 70% D_2O medium was used to inoculate 500 ml of 70% D_2O medium containing ^{15}N-labeled ammonium chloride and uniformly ^{13}C-labeled D-glucose. The protein was purified with size-exclusion chromatography, giving a final yield of 45 mg/l. The protein solution was concentrated to 30 mg/ml in 70% D_2O, then the protein solution was crystallized using the same procedure as for the H/D exchanged GB1.

Solid-State NMR experiments

Most solid-state NMR experiments were conducted on a Bruker Avance III HD 600 MHz (14.1 T) spectrometer using a 3.2 mm MAS probe, supplemented with data measured on a 400 MHz (9.4 T) spectrometer using a 4 mm MAS probe. Samples were spun at 15 or 20 kHz on the 600 MHz spectrometer and 10 kHz on the 400 MHz spectrometer (Table 1). ^{13}C chemical shifts were referenced to the 38.48 ppm CH_2 peak of adamantane on the TMS scale (Morcombe and Zilm 2003). Typical ^{2}H rf field strengths were 62.5–71.4 kHz for both excitation and $^{\text{RESPIRATION}}$CP, and CP contact times range from 267 µs for rigid perdeuterated samples to 1.67 ms for dynamic and H/D exchanged samples. Most experiments were conducted at 273 K. ^{1}H TPPM decoupling (Bennett et al. 1995) at 62.5–71.4 kHz was applied for protonated samples. For perdeuterated Val and bacterial cellulose, ^{13}C linewidths and intensities were unaffected by ^{1}H decoupling, thus no ^{1}H decoupling was applied during ^{13}C detection. ^{2}H spins have much shorter relaxation times than ^{1}H or ^{13}C due to the large quadrupolar interaction, and recycle delays as short as 100 ms have been reported for ^{2}H–^{13}C correlation experiments (Shi and Rienstra 2016). For CDN-Val we measured an overall ^{2}H T_1 of 14 ± 2 ms and have used recycle delays as short as 125 ms without significant signal attenuation or sample heating. This amounts to a 16-fold increase in the number of scans per unit time compared to ^{1}H-based experiments at a recycle delay of 2.0 s. Without the time saving, ^{2}H–^{13}C CP has only 15% of the sensitivity of ^{1}H–^{13}C CP due to the sevenfold lower gyromagnetic ratio of ^{2}H compared to ^{1}H. With this fourfold sensitivity increase due to time saving, ^{2}H–^{13}C CP experiments have a relative sensitivity of 61% compared to ^{1}H–^{13}C CP experiments. Perdeuterated bacterial cellulose has a longer ^{2}H T_1 of ~500 ms due to the absence of dynamic methyl groups, thus we used recycle delays of 1.5 s for this sample.

^{2}H spectral simulations

^{2}H quadrupolar spinning sideband patterns were simulated using DMFit (Massiot et al. 2002) and then processed in MATLAB. Uncertainties in the quadrupolar coupling constants were extracted by comparing the root-mean-square deviation (RMSD) between the experimental and simulated spectral intensities with the root-mean-square (RMS) noise of the experimental spectra:

$$\tilde{I}_{i,\text{exp}} = I_{i,\text{exp}} \Big/ \sum_{i=1}^{n} I_{n,\text{exp}} \tag{1}$$

$$RMSD = \sqrt{\sum_{i=1}^{n} \left(\tilde{I}_{i,\text{exp}} - \tilde{I}_{i,sim}\right)^2} \tag{2}$$

$$RMS\ noise = \sqrt{\frac{1}{k}\sum_{i=1}^{k} \left(I_{k,\text{exp}}\right)^2} \Big/ I_{\text{max,exp}} \tag{3}$$

Here the intensity of the ith sideband is normalized to the integrated intensity of the spectrum, and k is the number of data points used for the RMS noise calculation. The reported coupling uncertainties include all couplings whose calculated spectra deviate from the experimental spectrum by less than twice the experimental RMS noise.

Table 1 Isotopic labeling schemes, experimental conditions and maximum ^{2}H–^{13}C transfer efficiencies of the samples used in this study

Samples	ν_r (kHz)	$^{\text{RESPIRATION}}$CP contact time (ms)	CP transfer efficiency (%)
^{13}C, ^{15}N, ^{2}H-labeled Val	15	0.53	51
^{2}Hβ-labeled Ala	10	1.00	33
^{13}C, ^{2}H-labeled bacterial cellulose	15	0.47	79
^{13}C-labeled H/D exchanged D-glucose	15	1.33	31
^{13}C-labeled H/D exchanged *Arabidopsis* cell wall	15	1.67	2.2
Uniformly ^{13}C,^{15}N- and 70% ^{2}H-labeled GB1	20	0.50	23
^{13}C, ^{15}N labeled and H/D exchanged GB1	15	1.33	3.3

Results and discussion

Optimal MAS frequencies and contact times for one- and two-bond ^{2}H–^{13}C $^{\text{RESPIRATION}}$CP transfer

We first consider the optimal choice of MAS frequency that will produce a sufficient number of sidebands for reporting the coupling strength without excessively lowering spectral sensitivity. The rigid-limit C_Q values of deuteroxyl and aliphatic deuterons are 190–300 and 170 kHz, respectively, with corresponding asymmetry parameters (η) of about 0.15 and 0 (Burnett and Muller 1971; Clymer and Ragle 1982; Hoyland 1968; Hunt and MaCkay 1974). The large range of rigid-limit values for deuteroxyl groups is due to the strong dependence of quadrupolar couplings on hydrogen-bond distances. For fast methyl three-site jumps, the quadrupolar couplings are reduced threefold due to the scaling factor $\left(3\cos^2\theta - 1\right)/2 = -0.33$ where $\theta = 109.5°$ between the C–D bond and the C–C motional axis. If additional torsional motions are present, the quadrupolar couplings will be further reduced. Thus, the MAS frequencies need to be chosen to reflect quadrupolar couplings in a wide range of 50–250 kHz.

Figure 2a shows simulated ^{2}H spectra for C_Q values of 50–250 kHz at $\eta = 0$ under 15 and 20 kHz MAS. At 20 kHz spinning, there are too few sidebands to report the quadrupolar couplings of methyl groups accurately, while at 10 kHz MAS (not shown), the number of spinning sidebands is too large for rigid moieties and reduces spectral sensitivity. Thus, we chose an intermediate MAS frequency of 15 kHz to measure the C_Q of both dynamic and rigid functional groups. At this MAS frequency, the spectral lineshapes are sensitive to small quadrupolar couplings down to order parameters of 0.20 for aliphatic deuterons (Fig. 2b). Figure 2c shows the dependence of the ^{2}H sideband patterns on η. Not until η exceeds 0.3 can we observe significant intensity differences in the sideband patterns. Since this value is much larger than the η of most biomolecules, below we consider $\eta = 0$ for C–D groups and $\eta = 0.15$ for O–D groups in spectral simulations, and focus on quantifying motionally averaged coupling constants, $\overline{C_Q}$. However, for anisotropic motions that result in large $\overline{\eta}$ (Schmidt-Rohr and Spiess 1994), we use the $\overline{\eta}$ value consistent with the specific motional model.

We next examined the contact time for one- and two-bond ^{2}H–^{13}C $^{\text{RESPIRATION}}$CP transfer. For bacterial cellulose and Val (Fig. 3a, b), the CD and CD_2 groups of cellulose and Val Cα and Cβ reached maximum intensity at 0.4–0.5 ms, which is in good agreement with the expected transfer times based on the one-bond ^{2}H–^{13}C dipolar coupling of 3.52 kHz and a 1.37-fold slower buildup for $^{\text{RESPIRATION}}$CP compared to regular CP (Jain et al. 2012). The Val methyl Cγ groups show a slower buildup with maximum intensities at ~1 ms, as expected due to the threefold reduction of ^{2}H–^{13}C dipolar couplings by methyl rotation.

Under the condition that the number, n_I, of source spins, I, greatly exceeds the number, n_S, of sink spins, S, the theoretical CP enhancement factor compared to direct polarization (DP) is the ratio of the gyromagnetic ratios of the two spins, γ_I/γ_S. Thus, ideal $^{\text{RESPIRATION}}$CP transfer from ^{2}H ($\gamma = 6.5$ MHz/T) to ^{13}C ($\gamma = 10.7$ MHz/T) should have a theoretical "enhancement" factor of 0.61. We define the polarization transfer efficiencies, $\eta_{D\to C}$, as the ratio of the measured ^{2}H–^{13}C $^{\text{RESPIRATION}}$CP enhancement factor to this theoretical enhancement factor. For C–D deuterated samples (Fig. 3a–c), the experimental enhancement factor was evaluated as the ratio of the $^{\text{RESPIRATION}}$CP intensity $I_{D\to C}$ to the direct polarization (DP) intensity, I_C (Eq. 4).

$$\eta_{D\to C,C} = \frac{\gamma_C}{\gamma_D}\frac{I_{D\to C}}{I_C} \tag{4}$$

The ^{13}C DP spectra were measured with a single scan for perdeuterated rigid molecules to avoid slow ^{13}C T_1 relaxation. For protonated and H/D exchanged samples, the enhancement factors were measured as the ratio of the ^{2}H–^{13}C $^{\text{RESPIRATION}}$CP intensities to the ^{1}H–^{13}C ramp CP intensities (Metz et al. 1994) (Eq. 5). In this case, the theoretical enhancement factor of ^{1}H–^{13}C CP is included to ensure that these transfer efficiencies can be compared with the values obtained using DP as the reference:

$$\eta_{D\to C,HC} = \frac{\gamma_C}{\gamma_D}\frac{\gamma_H}{\gamma_C}\frac{I_{D\to C}}{I_{H\to C}} = \frac{\gamma_H}{\gamma_D}\frac{I_{D\to C}}{I_{H\to C}} \tag{5}$$

When n_I is not much larger than n_S, the transfer efficiency is scaled by $n_I/(n_S + n_I)$. For uniformly ^{13}C-labeled amino acids and carbohydrates, n_H is typically 2–3 times that of n_C. Thus, the theoretical ^{2}H–^{13}C transfer efficiency is 0.67–0.75 times the value obtained in the $n_I \gg n_S$ limit. Relaxation effects and experimental imperfections further reduce the transfer efficiency. The measured $^{\text{RESPIRATION}}$CP transfer efficiency for perdeuterated bacterial cellulose and Val is 50–80%, indicating that the one-bond ^{2}H–^{13}C polarization transfer is highly efficient.

To exclusively measure the spectra of deuterons that are directly bonded to carbon, we chose a CP contact time of 0.27 ms, which is shorter than the time for maximum one-bond polarization transfer in order to minimize the influence of deuterons two or three bonds away from the ^{13}C. The Val CO buildup curve (Fig. 3b) shows that the transfer efficiency is only 1% at 0.27 ms and reaches only 5% by 3 ms, which is negligible compared to the one-bond transfer efficiency.

CDN-labeled Val shows lower Cγ intensities than Cα and Cβ intensities for a range of $^{\text{RESPIRATION}}$CP contact

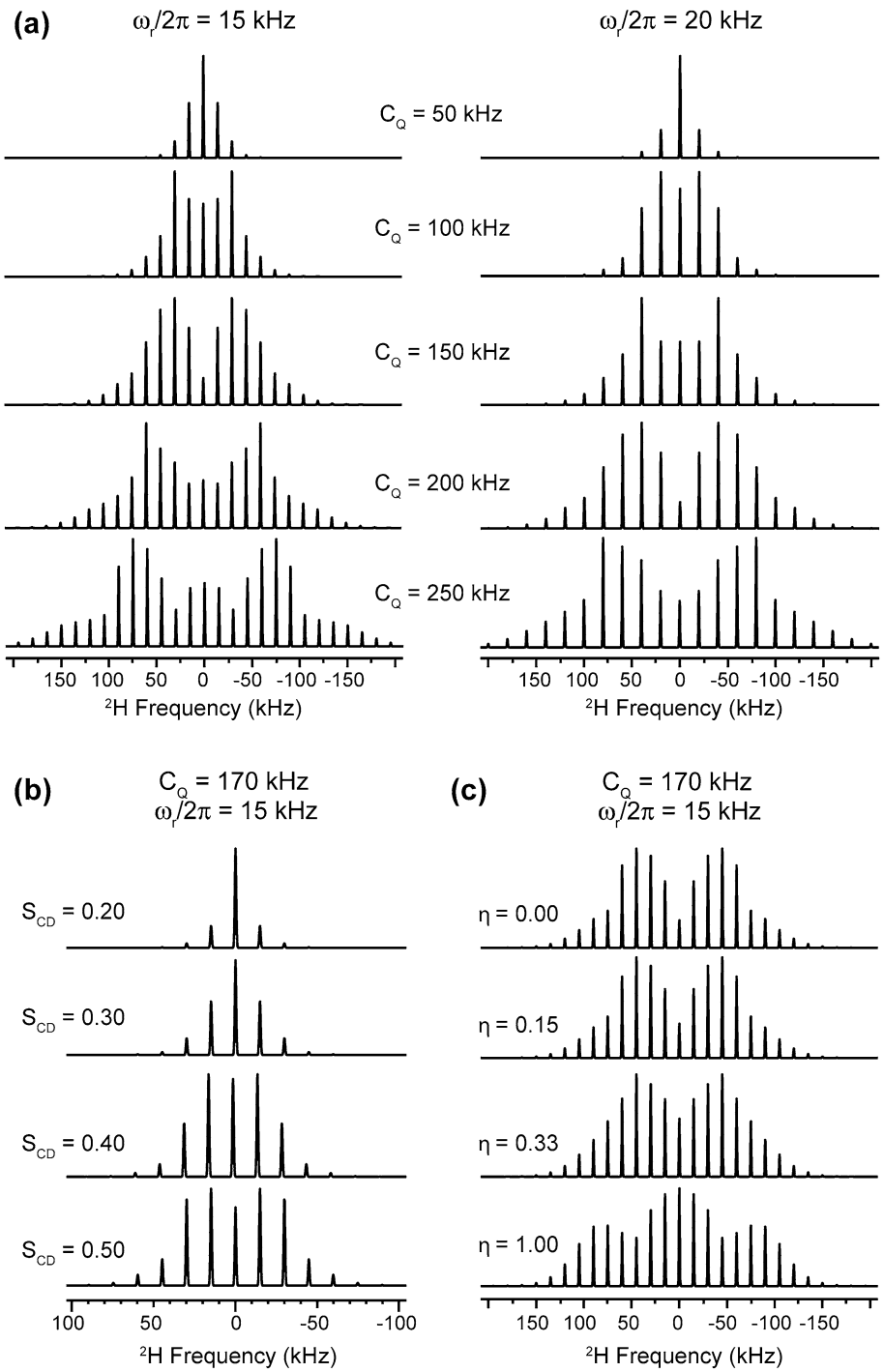

Fig. 2 Simulated ^{2}H quadrupolar spectra for varying quadrupolar coupling constants, MAS frequencies, and asymmetry parameters. **a** Simulated spectra for 15 and 20 kHz MAS for C_Q values from 50 to 250 kHz. **b** Simulated spectra for C–D order parameters from 0.20 to 0.50. **c** Simulated spectra as a function of η for $C_Q = 170$ kHz

times, indicating that methyl-rotation averaging of the ^{2}H–^{13}C dipolar couplings outweighs the larger number of deuterons to make ^{2}H–^{13}C polarization transfer less efficient. This differs from ^{1}H–^{13}C CP, which typically gives higher intensities for methyl carbons than CH and CH_2 carbons. We hypothesize that the lower efficiency of ^{2}H–^{13}C $^{\text{RESPIRATION}}$CP compared to ^{1}H–^{13}C CP for methyl groups is due to the presence of ^{1}H–^{1}H spin diffusion but the absence of ^{2}H–^{2}H spin diffusion. The former replenishes the ^{1}H magnetization for repeated polarization transfer to ^{13}C, thus increasing the methyl ^{13}C intensities despite the reduction of ^{1}H–^{13}C dipolar coupling by motion.

Deuterons introduced by H/D exchange can only be detected through two-bond polarization transfer to ^{13}C. Based on standard covalent bond angles and bond lengths of 0.96 Å for O–D, 1.09 Å for C–D, 1.43 Å for C–O, and 1.54 Å for C–C, the two-bond ^{2}H–(O)–^{13}C dipolar coupling is 5.9 times weaker than the one-bond ^{2}H–^{13}C dipolar

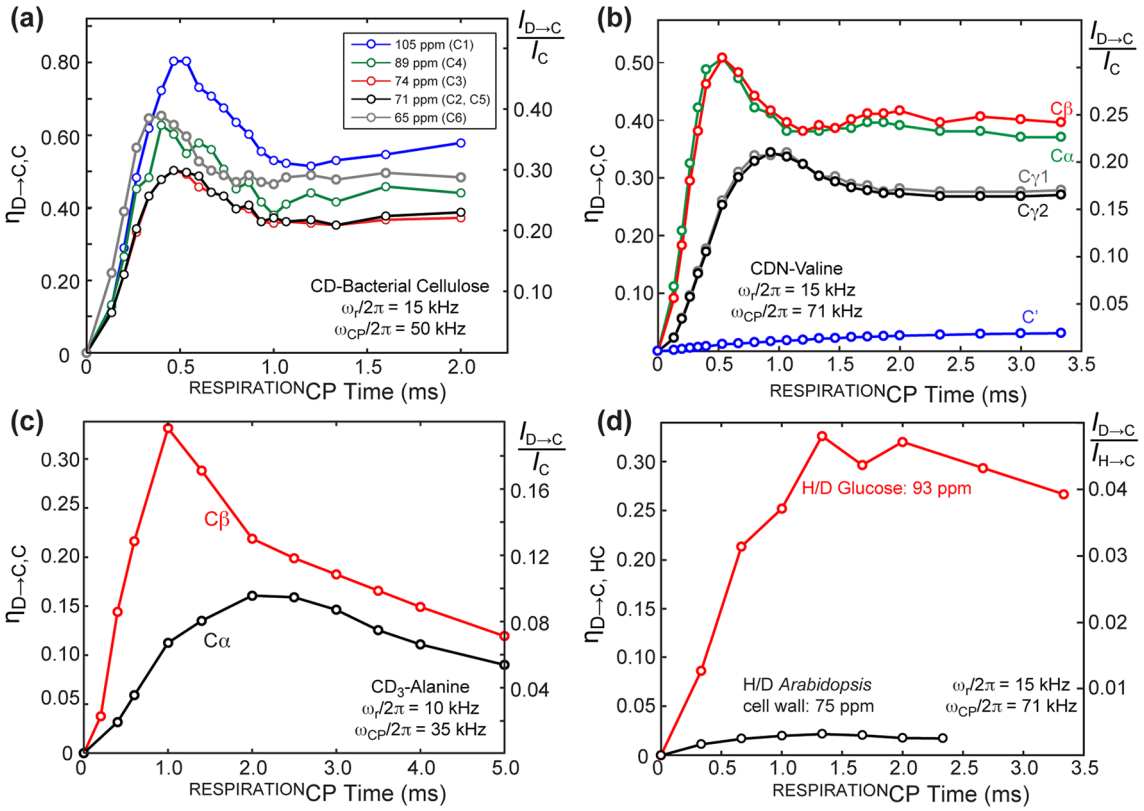

Fig. 3 ^{2}H–^{13}C polarization transfer efficiencies, $\eta_{D\rightarrow C}$, as a function of $^{\text{RESPIRATION}}$CP contact time for one-bond ^{13}C–^{2}H and two-bond ^{13}C–O–^{2}H spin systems. The transfer efficiencies, indicated on the left *y-axis*, are related to the enhancement factors $I_{D\rightarrow C}/I_C$ or $I_{D\rightarrow C}/I_{H\rightarrow C}$, shown on the right *y-axis*, according to Eqs. 4 and 5. **a** Polarization transfer of ^{2}H, ^{13}C-labeled bacterial cellulose. **b** Polarization transfer of CDN-labeled Val. **c** Polarization transfer of ^{2}Hβ-labeled Ala. **d** Polarization transfer of ^{13}C-labeled and H/D exchanged D-glucose and *Arabidopsis* cell walls. The data were obtained under 15 or 10 kHz MAS with the indicated short-pulse $^{\text{RESPIRATION}}$CP field strengths

coupling, while the two-bond ^{2}H–(C)–^{13}C dipolar coupling is 7.8 times weaker, thus requiring longer contact times compared to directly bonded deuterons. Methyl-deuterated Ala allowed the comparison of one-bond and two-bond ^{2}H–^{13}C transfers through the Cβ and Cα signals (Fig. 3c): the two-bond transfer to Cα peaked at a contact time of 2.0 ms, while the one-bond transfer to Cβ reached maximum intensity at 1.0 ms.

For H/D exchanged and ^{13}C-labeled D-glucose, maximum $^{\text{RESPIRATION}}$CP transfer is observed at a contact time of 1.3 ms (Fig. 3d). Five of twelve hydrogens in glucose are exchanged to deuterons, while each glucose unit in perdeuterated cellulose contains ten deuterons, thus the H/D exchanged glucose is expected to have about half the $^{\text{RESPIRATION}}$CP sensitivity of perdeuterated cellulose. The observed maximum $^{\text{RESPIRATION}}$CP efficiency for H/D exchanged glucose is 32%, which is indeed about half the transfer efficiency of perdeuterated cellulose (80%), in good agreement with prediction. Compared to H/D exchanged Glucose, the ^{13}C-labeled and H/D exchanged *Arabidopsis* primary cell wall gave significantly lower ^{2}H-^{13}C $^{\text{RESPIRATION}}$CP transfer efficiency of 2.2% at a CP contact time of 1.7 ms. This low efficiency can be attributed to the complex structures of the cell wall and the sequestration of some of the polysaccharides from water.

Minimum rf field strengths for indirect detection of undistorted ^{2}H quadrupolar spectra

To assess the minimum ^{2}H rf field strengths required to produce undistorted ^{2}H spectra, we measured the ^{2}H–^{13}C correlation spectra of CDN-Val and CD_3-labeled Ala at ^{2}H rf fields of 62.5, 50, and 35 kHz for the rotor-echo pulses. Figure 4 shows a representative 2D spectrum and ^{2}H cross sections of Val Cα and $C\gamma_1$. All spectra were measured using 62.5 kHz of RESPIRATION-4 ^{2}H excitation pulses, a CP contact time of 267 μs, and 90° flip angles for the short pulses. It can be seen that the 62.5 and 50 kHz $^{\text{RESPIRATION}}$CP pulses produced identical ^{2}H quadrupolar spectra while the 35 kHz $^{\text{RESPIRATION}}$CP pulses showed lower intensities for the outer sidebands while higher intensities for the ±1 and ±2 sidebands for Cα and the ±1

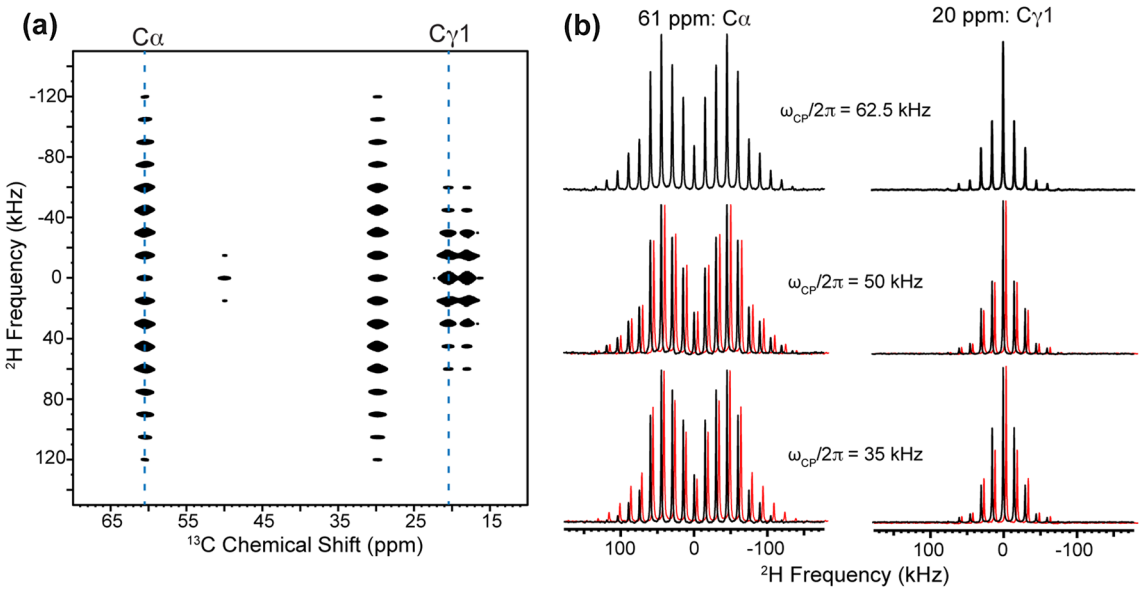

Fig. 4 **a** Representative 2D ^{2}H–^{13}C correlation spectrum of mixed CDN-labeled Val and ^{2}Hβ-labeled Ala, measured under 15 kHz MAS with a $^{\text{RESPIRATION}}$CP field strength of 62.5 kHz. **b** ^{2}H cross sections of Val Cα and Cγ as a function of the short-pulse $^{\text{RESPIRATION}}$CP field strength. The 62.5 kHz cross sections (*red*) are overlaid with the 50 and 35 kHz cross sections to illustrate differences in sideband intensities. The 35 kHz spectrum shows intensity distortions compared to the 62.5 and 50 kHz spectra

sidebands for $C\gamma_1$, indicating non-uniform excitation of the quadrupolar spectra. Thus, a minimum rf field of 50 kHz is required in the $^{\text{RESPIRATION}}$CP block to obtain undistorted quadrupolar spectra. Adiabatic $^{\text{RESPIRATION}}$CP has been shown to enhance ^{2}H–^{13}C magnetization transfer at low rf field strengths; however, $^{\text{RESPIRATION}}$CP with 50 kHz rf field still outperforms adiabatic $^{\text{RESPIRATION}}$CP at 20 kHz field strength (Jain et al. 2014).

^{2}H–^{13}C correlation spectra of bacterial cellulose—hydroxymethyl motion

High-resolution structures of crystalline Iα and Iβ cellulose have been extensively characterized using X-ray and neutron diffraction (Nishiyama et al. 2002, 2003) and solid-state NMR (Kono and Numata 2006; Kono et al. 2002; Masuda et al. 2003). *Acetobacter xylinus* cellulose is one of the most commonly studied sources of Iα cellulose. Recently, O'Neill and coworkers developed a method for growing deuterated bacterial cellulose for neutron scattering studies (O'Neill et al. 2015). Together with ^{13}C labeling, the ^{2}H-labeled bacterial cellulose presents an excellent model system for probing cellulose dynamics using ^{2}H–^{13}C correlation NMR. Polymer motions in bacterial cellulose composites with pectins, graphene oxide, and carboxymethyl cellulose have been investigated (Kačuráková et al. 2002; Sanchis et al. 2017), but the dynamics of hydrated bacterial cellulose alone has not been reported. Perdeuterated and H/D exchanged bacterial cellulose contains 7 C–D groups and 3 O–D groups per glucose unit. The complete absence of protons means that the ^{2}H–^{13}C $^{\text{RESPIRATION}}$CP spectrum should have the same intensity pattern as the ^{13}C DP spectrum, as is indeed observed (Fig. 5a, b). Consistent with previous SSNMR data (Atalla and VanderHart 1984; Earl and VanderHart 1981; Wang and Hong 2016), two sets of C4 and C6 peaks are resolved: the stronger C4 and C6 peaks at 88.7 and 64.8 ppm can be assigned to well ordered interior (*i*) cellulose, while the weaker signals at 83.4 and 61.3 ppm can be assigned to disordered cellulose on the surface (*s*) of the microfibril. The low intensities of the surface cellulose peaks indicate large diameters of the microfibril. Figure 5c shows the 2D ^{2}H–^{13}C correlation spectrum measured with a short $^{\text{RESPIRATION}}$CP contact time of 267 μs so that the ^{2}H dimension mainly reflects the C–D quadrupolar couplings. All ^{2}H cross sections (Fig. 5d) exhibit rigid-limit C_Q values of 170 kHz (Burnett and Muller 1971), except for sC6, which has a narrower intensity envelope indicative of weaker quadrupolar couplings.

C6 is the only carbon outside the pyranose ring (Fig. 5a), thus *trans-gauche* isomerization around the C5–C6 bond is possible. The motionally averaged $\overline{C_Q}$ and $\overline{\eta}$ values of a CD_2 group undergoing *trans-gauche* isomerization can be calculated (Palmer et al. 1996) by considering the motionally averaged quadrupolar coupling tensor. One principal axis of the average tensor bisects the angle between the initial and final C6–D vector, the second principal axis is perpendicular to this bisector in the plane of the initial and final C6–D vectors, while the third principal axis is

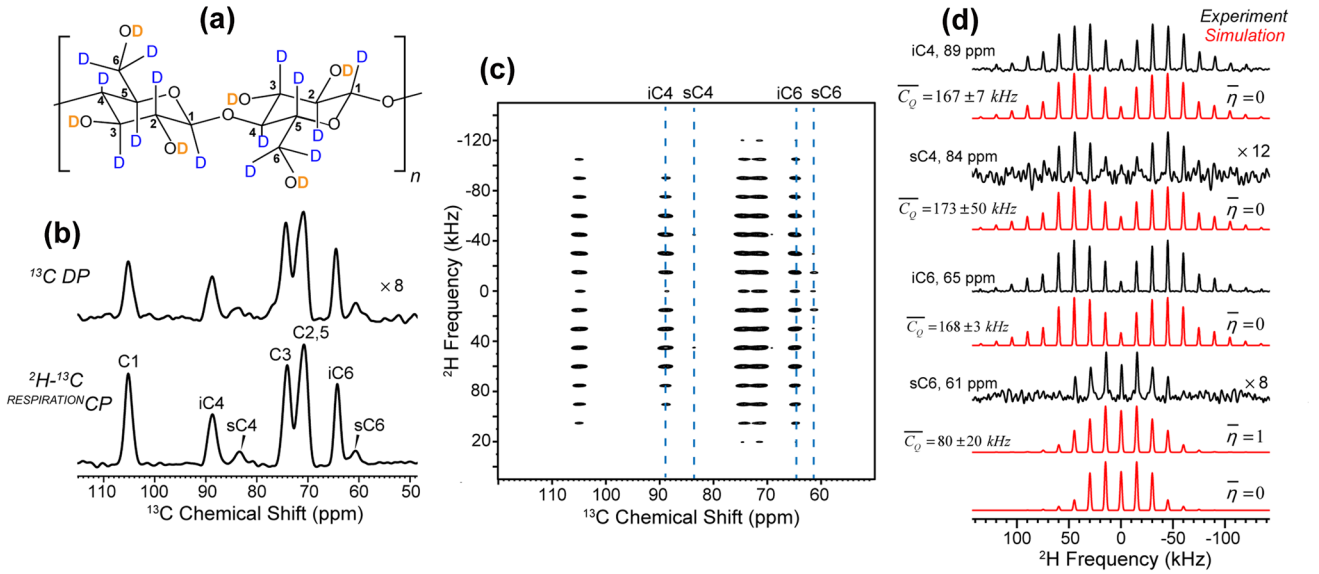

Fig. 5 2D ^{2}H–^{13}C correlation spectra of ^{2}H, ^{13}C-labeled bacterial cellulose. **a** Chemical structure of cellulose. **b** The ^{2}H–^{13}C ^{RESPIRATION}CP spectrum has the same intensity distribution as the ^{13}C DP spectrum. **c** 2D ^{2}H–^{13}C correlation spectrum, measured under 15 kHz MAS. **d** ^{2}H cross sections of iC4, sC4, iC6, and sC6. Best-fit simulations (*red*) for $\bar{\eta}=1$ indicate that the surface cellulose C6 is motionally averaged at 293 K. Alternative fit assuming $\bar{\eta}=0$ gives a similar $\overline{C_Q}$ value, but does not match the experimental spectrum, indicating that the spectrum is sensitive to the asymmetry parameter of motion

normal to this plane. The principal values associated with these axes can be calculated using $\overline{\omega_n} = \frac{1}{2}C_Q\left(3\cos^2\theta_n - 1\right)$, where θ_n is the angle between the individual principal axes and the motional axis. For tetrahedral geometry, $\theta_1 = 35.3°$, $\theta_2 = 54.7°$, and $\theta_3 = 90°$, yielding a motionally averaged $\overline{C_Q} = 0.5C_Q$ and $\overline{\eta} \equiv \left(\overline{\omega_2} - \overline{\omega_3}\right)/\overline{\omega_1} = 1$.

Using $\overline{\eta} = 1$, we simulated the surface cellulose C6 ^{2}H quadrupolar pattern and obtained a best fit at $\overline{C_Q} = 80 \pm 20\ kHz$ (Fig. 5d). This corresponds to an order parameter of 0.47, in excellent agreement with the expected scaling of 0.50 for *trans-gauche* isomerization. Thus, the ^{2}H spectra indicate unambiguously that surface cellulose chains undergo fast *trans-gauche* isomerization around the C5–C6 bond. This motion persists down to 248 K (data not shown), suggesting a low energy barrier. Importantly, this motion is only observed for the disordered surface cellulose, while the interior crystalline cellulose C6 peak at 64.8 ppm shows a rigid-limit quadrupolar coupling spectrum up to 313 K, the highest temperature used for these experiments, indicating that the torsional motion is absent for glucan chains within the microfibril.

^{2}H–^{13}C correlation spectra of H/D exchanged glucose and *Arabidopsis* cell wall

The applicability of ^{2}H–^{13}C ^{RESPIRATION}CP for H/D exchanged molecules is demonstrated using D-glucose and *Arabidopsis* cell walls. The ^{1}H–^{13}C CP spectrum of ^{13}C-labeled and H/D exchanged D-glucose shows two sets of resonances, corresponding to α-D-glucose and β-D-glucose (Fig. 6a). Although C2, C3, and C4 peaks show partial overlap, the two C5 peaks can be resolved, and their intensities are reduced by >40% in the ^{2}H–^{13}C ^{RESPIRATION}CP spectrum, consistent with the fact that C5 is the only carbon in glucose without a directly bonded deuteroxyl group. The ^{RESPIRATION}CP sensitivity of this H/D exchanged sample is lower than that of perdeuterated compounds (Fig. 3), as expected because of the two-bond ^{2}H–^{13}C polarization transfer and the smaller number of ^{2}H spins. The indirect dimension of the 2D correlation spectrum shows a broad intensity envelope for all patterns, indicating large quadrupolar couplings and the lack of conformational dynamics. Assuming an asymmetry parameter of 0.15, we can fit these sideband patterns using C_Q values of 190–200 kHz (Fig. 6c), which are consistent with literature values for hydrogen-bonded rigid deuteroxyl quadrupolar couplings (Clymer and Ragle 1982; Hunt and MaCkay 1974).

Figure 7a shows the ^{1}H–^{13}C CP spectrum of H/D exchanged *Arabidopsis* cell walls, where ^{13}C chemical shifts are assigned based on previous 2D correlation spectra (Dick-Pérez et al. 2011; Wang et al. 2015). With a ^{2}H–^{13}C ^{RESPIRATION}CP contact time of 1.7 ms, the ^{13}C intensities are 0.17% of the ^{1}H–^{13}C CP spectral intensities (Fig. 7a). This sensitivity is about 15-fold lower than that of H/D exchanged glucose. Since the ^{RESPIRATION}CP matching conditions are quite robust, this low efficiency most likely results from low water accessibility of many

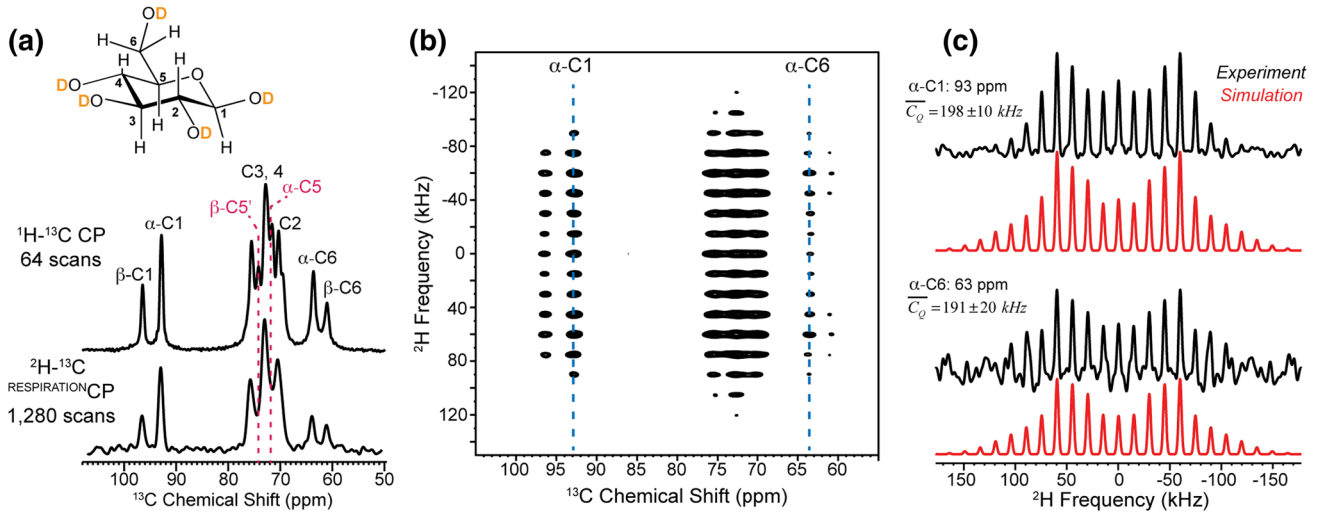

Fig. 6 ^{2}H–^{13}C correlation spectra of ^{13}C-labeled and H/D exchanged D-glucose. **a** Comparison of ^{1}H–^{13}C CP and ^{2}H–^{13}C $^{\text{RESPIRATION}}$CP spectra. The C5 signal is suppressed in the ^{2}H–^{13}C CP spectrum due to its lack of directly bonded O–D. **b** 2D ^{2}H–^{13}C correlation spectrum, measured under 15 kHz MAS. **c** ^{2}H cross sections of C1 (93 ppm) and C6 (64 ppm). Best-fit simulations give rigid-limit O–D quadrupolar couplings

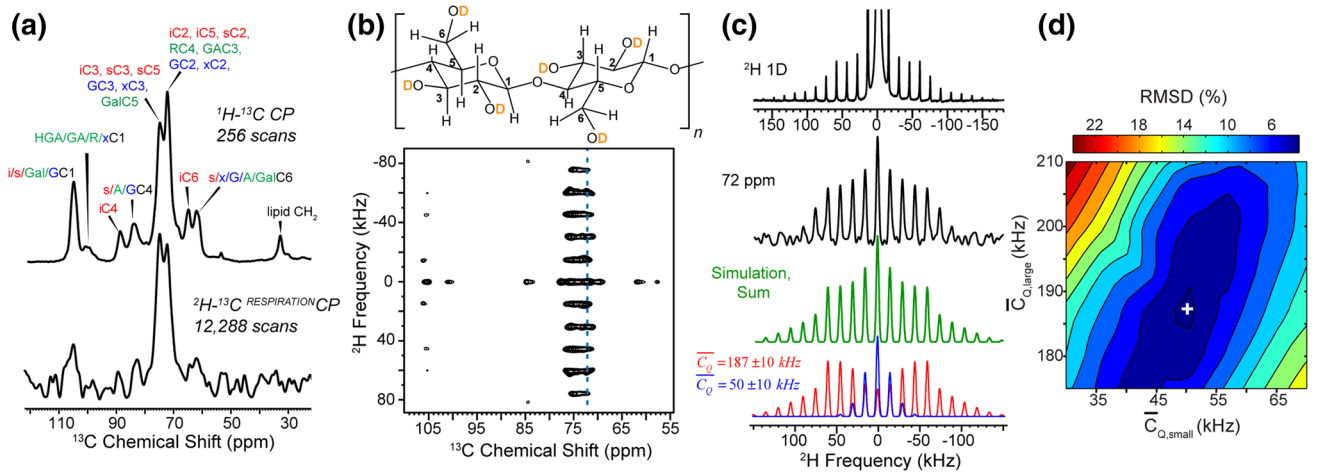

Fig. 7 ^{2}H–^{13}C correlation spectra of ^{13}C-labeled and H/D exchanged *Arabidopsis* cell wall. **a** Comparison of ^{1}H–^{13}C CP and ^{2}H–^{13}C $^{\text{RESPIRATION}}$CP spectra. **b** 2D ^{2}H–^{13}C correlation spectrum, measured under 15 kHz MAS at 273 K. Cellulose structure is shown. **c** 72-ppm ^{2}H cross sections of C2 and C5. Best-fit simulation was obtained with two $\overline{C_Q}$ values of 187 and 50 kHz with weighting factors of 74 and 26%, respectively. For comparison, the 1D ^{2}H MAS spectrum with RESPIRATION-4 excitation is shown. **d** 2D RMSD contour plot for determining the best-fit quadrupolar couplings (marked by a *white cross*) for the C2 and C5 cross section

polysaccharides in the cell wall and motional averaging of the ^{2}H-^{13}C dipolar couplings. The wall polysaccharides form a complex network where the matrix polysaccharides are preferentially hydrated while cellulose is not (White et al. 2014). Moreover, pectins are highly dynamic, with C–H order parameters of 0.46–0.55 (Wang et al. 2015), which further reduce the polarization transfer efficiency. Figure 7b shows the 2D ^{2}H–^{13}C correlation spectrum measured at 273 K. At this temperature, chemical exchange is known to be slow (Liepinsh and Otting 1996), as confirmed by the absence of a large isotropic peak in the ^{2}H dimension of the 2D spectrum. Due to the low sensitivity of the 2D spectrum, we focus on the ^{2}H cross sections of the 72-ppm and 75-ppm peaks, which result from a mixture of C2, C3 and C5 of cellulose, xyloglucan, and pectins. Direct inspection indicates that the spectral pattern cannot be fit by a single set of $\overline{C_Q}$ and $\overline{\eta}$ values (Fig. 7c), but is a superposition of a large and a small quadrupolar coupling, $\overline{C_{Q,large}}$ and $\overline{C_{Q,small}}$. Thus, we fit the spectrum using a two-component model

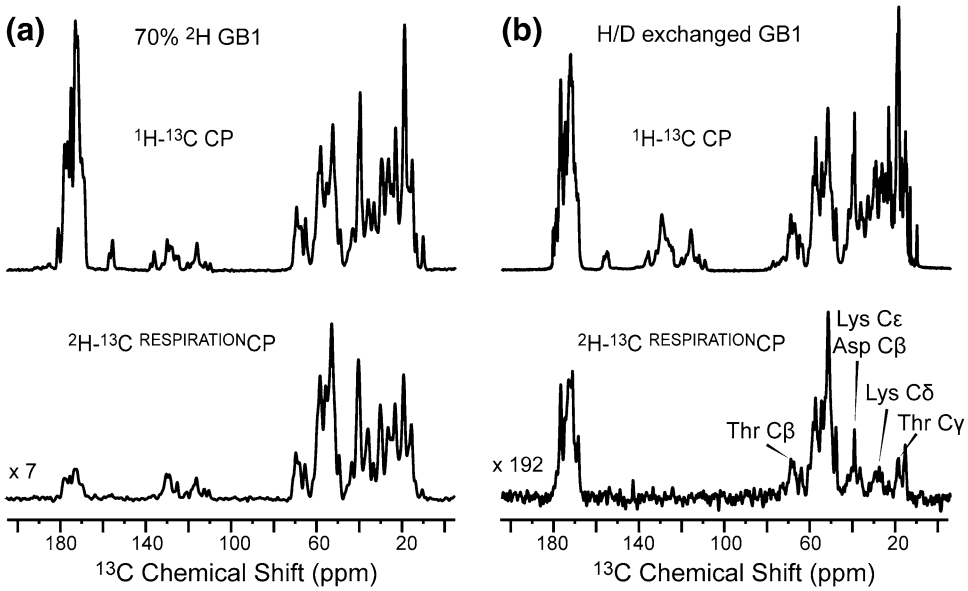

Fig. 8 **a** ^{1}H–^{13}C CP and ^{2}H–^{13}C $^{\text{RESPIRATION}}$CP spectra of uniformly ^{13}C,^{15}N labeled and 70% ^{2}H-labeled GB1. **b** ^{1}H–^{13}C CP and ^{2}H–^{13}C $^{\text{RESPIRATION}}$CP spectra of ^{13}C-labeled and H/D exchanged GB1. The different intensity patterns of the ^{2}H–^{13}C spectra are consistent with the distinct deuteron distributions in the two samples

in which $\overline{C_{Q,l\arg e}}$ varies from 173 to 220 kHz and $\overline{C_{Q,small}}$ varies from 23 to 77 kHz. To determine the percentages of the two components, we fit the 4th to 6th sidebands to $\overline{C_{Q,l\arg e}}$ with $\eta = 0.15$, since mobile components with $\overline{C_Q}$ less than ~75 kHz contribute negligible intensities to these outer sidebands. The simulated spectrum for the large-coupling component was then subtracted from the experimental spectrum to obtain the coupling of the mobile component. The percentages of the two components are obtained from the integrated intensities of each simulated spectrum. We found a global best fit at $\overline{C_{Q,l\arg e}} = 187 \pm 10$ kHz and $\overline{C_{Q,small}} = 50 \pm 10$ kHz, with relative intensities of 74 and 26%, respectively (Fig. 7d).

Rigid-limit quadrupolar couplings of O–D groups are sensitive to hydrogen bonding. Hunt and Mackay showed that the deuteroxyl C_Q decreases with increasing hydrogen-bond length between the deuteron and the acceptor r according to the equation $C_Q = 328 - 643/r^3$, where r is in the Å unit (Hunt and MaCkay 1974). Thus, a non-hydrogen-bonded O–D group has a maximum quadrupolar coupling of 328 kHz. Joint X-ray and neutron diffraction analysis of cellulose showed that the positions of O–D…O hydrogens have significant uncertainties for both Iα and Iβ cellulose (Nishiyama et al. 2002, 2003), but the O3–D3···O5 hydrogen bonds are well defined. Therefore, we used the D3···O5 hydrogen-bond length for estimating the rigid-limit quadrupolar coupling. Since the cellulose conformation in the *Arabidopsis* cell wall is not exclusively Iβ or Iα (Wang et al. 2016c), we used the C3–D3···O5 hydrogen-bond length range of 1.75–2.07 Å found in the two allomorphs to obtain a rigid-limit quadrupolar coupling of 230 ± 25 kHz. Based on this value, the measured coupling constants indicate an O–D order parameter (S_{OD}) of 0.81 for the rigid component and 0.22 for the dynamic component, which are assigned to cellulose and pectins, respectively. Interestingly, the pectin S_{OD} values are significantly smaller than the S_{CH} values measured using ^{13}C–^{1}H DIPSHIFT experiments (Dick-Pérez et al. 2011; Wang and Hong 2016; Wang et al. 2012; Williams et al. 2015). Although the ^{2}H quadrupolar coupling are more sensitive to small-amplitude motions than ^{13}C–^{1}H dipolar couplings, we consider this order parameter difference to be larger than the uncertainties of these two techniques, and attribute the lower S_{OD} values to the presence of additional motions in the deuteroxyl groups relative to the CD groups in matrix polysaccharides.

^{2}H–^{13}C polarization transfer in perdeuterated and H/D exchanged protein GB1

We finally test ^{2}H–^{13}C polarization transfer on microcrystalline GB1, whose structure is well known (Franks et al. 2005; Gallagher et al. 1994; Gronenborn et al. 1991; Schmidt et al. 2007). A 70% deuterated GB1 and a H/D exchanged GB1 provided two complementary model compounds for comparing the efficiencies of one-bond and multi-bond ^{2}H–^{13}C polarization transfer. Figure 8a compares the ^{13}C spectra of 70% deuterated GB1 measured with ^{1}H–^{13}C CP and ^{2}H–^{13}C $^{\text{RESPIRATION}}$CP. Due to the statistical ^{2}H labeling (Nand et al. 2012), the Cα and Cβ region has similar intensity distributions between the ^{1}H and ^{2}H polarized spectra, but the per-scan sensitivity is higher for ^{1}H–^{13}C CP as expected. In comparison, the carbonyl and methyl carbons have relatively reduced

intensities in the ^{2}H–^{13}C transferred spectrum, consistent with the lack of directly bonded deuterons and motional averaging.

For H/D exchanged GB1, a qualitatively different ^{2}H–^{13}C CP spectrum, with preferential enhancement of the CO and Cα signals, is observed (Fig. 8b), as expected because of the proximity of these carbons to exchangeable amide hydrogens. Moreover, the spectrum also exhibits the signals of carbons that are adjacent to labile sidechain OH and NH groups such as Thr, Lys, Asp, Glu, Asn, and Gln, which are assigned based on the known chemical shifts of this protein (Fig. 8b).

Conclusion

These data demonstrate that $^{\text{RESPIRATION}}$CP based ^{2}H–^{13}C correlation experiments can be applied to carbohydrates as well as proteins, and can be used to detect both one-bond C–D and two-bond C–(C)–D and C–(O)–D groups. We have examined the ^{2}H–^{13}C polarization transfer times for the different chemical groups and investigated the optimal MAS frequencies and ^{2}H rf field strengths required to detect undistorted ^{2}H spectra that can yield dynamical information. Accurate ^{2}H quadrupolar sideband patterns can be measured using moderate ^{2}H rf field strengths of ~50 kHz at an optimal MAS frequency of 15 kHz.

Our data show that even in the highly crystalline bacterial cellulose, fast *trans-gauche* isomerization is present at the C6 hydroxymethyl group of the disordered surface glucan chains, while glucan chains in the microfibril interior are fully immobilized by chain packing and hydrogen bonding. In *Arabidopsis* primary cell walls, the matrix polysaccharides show highly mobile O–D groups, whose order parameters are significantly lower than the C–H dipolar order parameters, indicating the presence of additional motion of the C–O bonds. Our data on the H/D exchanged glucose, plant cell wall, and GB1 indicate that ^{2}H magnetization can be readily transferred to ^{13}C spins that are two bonds away, thus allowing ^{2}H–^{13}C correlation NMR to be used not only for studying molecular motion but also for probing water accessibility of complex biological macromolecules with site resolution.

Acknowledgements This work is partially supported by NIH grant GM088204 to M. H. The plant cell wall and bacterial cellulose portion of the work was supported by the Center for Lignocellulose Structure and Formation, an Energy Frontier Research Center funded by the U.S. Department of Energy, Office of Science, Basic Energy Sciences under Award # DE-SC0001090.

References

Akbey Ü et al (2014) Quadruple-resonance magic-angle spinning nmr spectroscopy of deuterated solid proteins. Angew Chem Int Edit 53:2438–2442

Andreas LB, Le Marchand T, Jaudzems K, Pintacuda G (2015) High-resolution proton-detected NMR of proteins at very fast MAS. J Magn Reson 253:36–49

Atalla RH, VanderHart DL (1984) Native cellulose: a composite of two distinct crystalline forms. Science 223:283–285

Bali G, Foston MB, O'Neill HM, Evans BR, He J, Ragauskas AJ (2013) The effect of deuteration on the structure of bacterial cellulose. Carbohyd Res 374:82–88

Bennett AE, Rienstra CM, Auger M, Lakshmi KV, Griffin RG (1995) Heteronuclear decoupling in rotating solids. J Chem Phys 103:6951–6958

Burnett L, Muller B (1971) Deuteron quadrupole coupling constants in three solid deuterated paraffin hydrocarbons: C_2D_6, C_4D_{10}, C_6D_{14}. J Chem Phys 55:5829–5831

Clymer JW, Ragle JL (1982) Deuterium quadrupole coupling in methanol, salicyclic acid, catechol, resorcinol, and hydroquinone. J Chem Phys 77:4366–4373

Cobo MF, Achilles A, Reichert D, Deazevedo ER, Saalwächter K (2012) Recoupled separated-local-field experiments and applications to study intermediate-regime molecular motions. J Magn Reson 221:85–96

Dick-Perez M, Wang T, Salazar A, Zabotina OA, Hong M (2012) Multidimensional solid-state NMR studies of the structure and dynamics of pectic polysaccharides in uniformly 13C-labeled Arabidopsis primary cell walls. Magn Reson Chem 50:539–550

Dick-Pérez M, Zhang Y, Hayes J, Salazar A, Zabotina OA, Hong M (2011) Structure and Interactions of plant cell-wall polysaccharides by two- and three-dimensional magic-angle-spinning solid-state NMR. Biochem-US 50:989–1000

Earl WL, VanderHart DL (1981) Observations by high-resolution carbon-13 nuclear magnetic resonance of cellulose I related to morphology and crystal structure. Macromolecules 14:570–574

Franks WT et al (2005) Magic-angle spinning solid-state NMR spectroscopy of the β1 immunoglobulin binding domain of protein G (GB1): ^{15}N and ^{13}C chemical shift assignments and conformational analysis. J Am Chem Soc 127:12291–12305

Frey MH, Opella SJ (1984) ^{13}C spin exchange in amino acids and peptides. J Am Chem Soc 106:4942–4945

Gallagher T, Alexander P, Bryan P, Gilliland GL (1994) Two crystal structures of the B1 immunoglobulin-binding domain of streptococcal protein G and comparison with NMR. BioChemistry 33:4721–4729

Gronenborn AM, Filpula DR, Essig NZ, Achari A, Whitlow M, Wingfield PT, Clore GM (1991) A novel, highly stable fold of the immunoglobulin binding domain of streptococcal protein G. Science 253:657–661

He J et al (2014) Controlled incorporation of deuterium into bacterial cellulose. Cellulose 21:927–936

Hologne M, Faelber K, Diehl A, Reif B (2005) Characterization of dynamics of perdeuterated proteins by MAS solid-state NMR. J Am Chem Soc 127:11208–11209

Hong M, Gross JD, Rienstra CM, Griffin RG, Kumashiro KK, Schmidt-Rohr K (1997) Coupling amplification in 2D MAS NMR and its application to torsion angle determination in peptides. J Magn Reson 129:85–92

Hou G, Byeon IJ, Ahn J, Gronenborn AM, Polenova T (2011) 1 H-13C/1 H-15N heteronuclear dipolar recoupling by R-symmetry sequences under fast magic angle spinning for dynamics analysis of biological and organic solids. J Am Chem Soc 133:18646–18655

Hoyland JR (1968) Ab initio bond-orbital calculations. I. Application to methane, ethane, propane, and propylene. J Am Chem Soc 90:2227–2232

Hunt MJ, MaCkay AL (1974) Deuterium and nitrogen pure quadrupole resonance in deuterated amino acids. J Magn Reson 15:402–414

Jain S, Bjerring M, Nielsen NC (2012) Efficient and robust heteronuclear cross-polarization for high-speed-spinning biological solid-state NMR spectroscopy. J Phys Chem Lett 3:703–708

Jain SK et al (2014) Low-power polarization transfer between deuterons and spin-1/2 nuclei using adiabatic $^{\text{RESPIRATION}}$CP in solid-state NMR. Phys Chem Chem Phys 16:2827–2830

Kačuráková M, Smith AC, Gidley MJ, Wilson RH (2002) Molecular interactions in bacterial cellulose composites studied by 1D FT-IR and dynamic 2D FT-IR spectroscopy. Carbohyd Res 337:1145–1153

Komatsu T, Kikuchi J (2013) Selective signal detection in solid-state NMR using rotor-synchronized dipolar dephasing for the analysis of hemicellulose in lignocellulosic biomass. J Phys Chem Lett 4:2279–2283

Kono H, Numata Y (2006) Structural investigation of cellulose I_a and I_b by 2D RFDR NMR spectroscopy: determination of sequence of magnetically inequivalent D-glucose units along cellulose chain. Cellulose 13:317–326

Kono H, Yunoki S, Shikano T, Fujiwara M, Erata T, Takai M (2002) CP/MAS ^{13}C NMR study of cellulose and cellulose derivatives. 1. Complete assignment of the CP/MAS ^{13}C NMR spectrum of the native cellulose. J Am Chem Soc 124:7506–7511

Lesage A, Steuernagel S, Emsley L (1998) Carbon-13 spectral editing in solid-state NMR using heteronuclear scalar couplings. J Am Chem Soc 120:7095–7100

Liepinsh E, Otting G (1996) Proton exchange rates from amino acid side chains—implications for image contrast. Magn Reson Med 35:30–42

Lu X, Zhang H, Lu M, Vega AJ, Hou G, Polenova T (2016) Improving dipolar recoupling for site-specific structural and dynamics studies in biosolids NMR: windowed RN-symmetry sequences. Phys Chem Chem Phys 18:4035–4044

Mao JD, Schmidt-Rohr K (2004) Separation of aromatic-carbon C-13 NMR signals from di-oxygenated alkyl bands by a chemical-shift-anisotropy filter. Solid State Nucl Magn 26:36–45

Mao J-D, Schmidt-Rohr K (2005) Methylene spectral editing in solid-state ^{13}C NMR by three-spin coherence selection. J Magn Reson 176:1–6

Massiot D et al. (2002) Modelling one- and two-dimensional solid-state NMR spectra. Mag Reson Chem 40:70–76

Masuda K, Adachi M, Hirai A, Yamamoto H, Kaji H, Horii F (2003) Solid-state ^{13}C and ^{1}H spin diffusion NMR analyses of the microfibril structure for bacterial cellulose. Solid State Nucl Mag Reson 23:198–212

Metz G, Wu XL, Smith SO (1994) Ramped-amplitude cross polarization in magic-angle-spinning NMR. J Magn Reson Series A 110:219–227

Morcombe CR, Zilm KW (2003) Chemical shift referencing in MAS solid state NMR. J Magn Reson 162:479–486

Munowitz M, Griffin R, Bodenhausen G, Huang T (1981) Two-dimensional rotational spin-echo nuclear magnetic resonance in solids: correlation of chemical shift and dipolar interactions. J Am Chem Soc 103:2529–2533

Nadaud PS, Helmus JJ, Höfer N, Jaroniec CP (2007) Long-range structural restraints in spin-labeled proteins probed by solid-state nuclear magnetic resonance spectroscopy. J Am Chem Soc 129:7502–7503

Nand D, Cukkemane A, Becker S, Baldus M (2012) Fractional deuteration applied to biomolecular solid-state NMR spectroscopy. J Biomol NMR 52:91–101

Nielsen NC, Bildso/e H, Jakobsen HJ, Levitt MH (1994) Double-quantum homonuclear rotary resonance: efficient dipolar recovery in magic-angle spinning nuclear magnetic resonance. J Chem Phys 101:1805–1812

Nishiyama Y, Langan P, Chanzy H (2002) Crystal structure and hydrogen-bonding system in cellulose Iβ from synchrotron X-ray and neutron fiber diffraction. J Am Chem Soc 124:9074–9082

Nishiyama Y, Sugiyama J, Chanzy H, Langan P (2003) Crystal structure and hydrogen bonding system in cellulose Iα from synchrotron X-ray and neutron fiber diffraction. J Am Chem Soc 125:14300–14306

O'Neill H et al (2015) Chapter six - production of bacterial cellulose with controlled deuterium–hydrogen substitution for neutron scattering studies. In: Zvi K (ed) Method Enzymol, vol 565. Academic Press, San Diego, pp 123–146

Palmer AG, Williams J, McDermott A (1996) Nuclear magnetic resonance studies of biopolymer dynamics. J Phys Chem 100:13293–13310

Pines A, Gibby MG, Waugh JS (1972) Proton-Enhanced nuclear induction spectroscopy. A method for high resolution NMR of dilute spins in solids. J Chem Phys 56:1776–1777

Reif B (2012) Deuterated peptides and proteins: structure and dynamics studies by MAS solid-state NMR. Methods Mol Biol 831:279–301

Sanchis MJ, Carsí M, Gómez CM, Culebras M, Gonzales KN, Torres FG (2017) Monitoring molecular dynamics of bacterial cellulose composites reinforced with graphene oxide by carboxymethyl cellulose addition. Carbohyd Polym 157:353–360

Schmidt HL, Sperling LJ, Gao YG, Wylie BJ, Boettcher JM, Wilson SR, Rienstra CM (2007) Crystal polymorphism of protein GB1 examined by solid-state NMR spectroscopy and X-ray diffraction. J Phys Chem B 111:14362–14369

Schmidt-Rohr K, Mao JD (2002) Efficient CH-group selection and identification in C-13 solid-state NMR by dipolar DEPT and H-1 chemical-shift filtering. J Am Chem Soc 124:13938–13948

Schmidt-Rohr K, Spiess HW (1994) Multidimensional Solid-State NMR and Polymers. Series vol., 1st edn. Academic Press, San Diego

Schmidt-Rohr K, Fritzsching KJ, Liao SY, Hong M (2012) Spectral editing of two-dimensional magic-angle-spinning solid-state NMR spectra for protein resonance assignment and structure determination. J Biomol NMR 54:343–353

Shi X, Rienstra CM (2016) Site-specific internal motions in GB1 protein microcrystals revealed by 3D ^{2}H–^{13}C–^{13}C solid-state NMR spectroscopy. J Am Chem Soc 138:4105–4119

Wang T, Hong M (2016) Solid-state NMR investigations of cellulose structure and interactions with matrix polysaccharides in plant primary cell walls. J Exp Bot 67:503–514

Wang T, Zabotina OA, Miller RC, Hong M (2012) Pectin-cellulose interactions in arabidopsis primary cell wall from two-dimensional magic-angle-spinning solid-state NMR. BioChemistry 51:9846–9856

Wang T, Salazar A, Zabotina OA, Hong M (2014) Structure and dynamics of brachypodium primary cell wall polysaccharides from two-dimensional ^{13}C solid-state nuclear magnetic resonance spectroscopy. Biochem-US 53:2840–2854

Wang T, Park YB, Cosgrove DJ, Hong M (2015) Cellulose-pectin spatial contacts are inherent to never-dried Arabidopsis primary cell walls: evidence from solid-state nuclear magnetic resonance. Plant Physiol 168:871–884

Wang T, Chen Y, Tabuchi A, Cosgrove DJ, Hong M (2016a) The target of β-expansin EXPB1 in maize cell walls from binding and solid-state NMR studies. Plant Physiol 172:2107–2119

Wang T, Phyo P, Hong M (2016b) Multidimensional solid-state NMR spectroscopy of plant cell walls. Solid State Nucl Mag 78:56–63

Wang T, Yang H, Kubicki JD, Hong M (2016c) Cellulose structural polymorphism in plant primary cell walls investigated by high-field 2D solid-state NMR spectroscopy and density functional theory calculations. Biomacromolecules 17:2210–2222

Wei D, Akbey Ü, Paaske B, Oschkinat H, Reif B, Bjerring M, Nielsen NC (2011) Optimal ^{2}H rf Pulses and ^{2}H–^{13}C cross-polarization methods for solid-state ^{2}H MAS NMR of perdeuterated proteins. J Phys Chem Lett 2:1289–1294

White PB, Wang T, Park YB, Cosgrove DJ, Hong M (2014) Water–polysaccharide interactions in the primary cell wall of *Arabidopsis thaliana* from polarization transfer solid-state NMR. J Am Chem Soc 136:10399–10409

Williams JK, Schmidt-Rohr K, Hong M (2015) Aromatic spectral editing techniques for magic-angle-spinning solid-state NMR spectroscopy of uniformly ^{13}C-labeled proteins. Solid State Nucl Mag 72:118–126

Wu XL, Burns ST, Zilm KW (1994) Spectral editing in CPMAS NMR. Generating subspectra based on proton multiplicities. J Magn Reson Series A 111:29–36